THE JOURNAL OF PHYSICAL CHEMISTRY C
A JOURNAL OF THE AMERICAN CHEMICAL SOCIETY



pubs.acs.org/JPCC
Article

# Graphene Structure Modification under Tritium Exposure: $^3$H Chemisorption Dominates over Defect Formation by $\beta^-$ Radiation

Alexandra Becker,* Genrich Zeller, Holger Lippold, Ismail Eren, Lara Rkaya Müller, Paul Chekhonin, Agnieszka Beata Kuc, Magnus Schlösser, and Cornelius Fischer

Cite This: J. Phys. Chem. C 2025, 129, 21995−22005



**ABSTRACT:** Potential structural modifications of graphene exposed to gaseous tritium are important for membrane-based hydrogen isotope separation. Previously, it has been reported that tritium−graphene interactions cause absorption as well as vacancy defects in graphene. In this work, we investigate the mechanism, which leads to the generation of the vacancy defects. We find that such modifications cannot be explained by electron irradiation alone. Instead, the tritium radicals remaining after the decay are the primary cause of the modification of the graphene surface, as confirmed by confocal Raman microscopy. The effect of the interaction of tritium atoms with the graphene surface exceeds that of electron irradiation at the average energy of the beta particles (5.7 keV). Compared to other studies, which investigated high electron doses in the absence of tritium, remarkably low concentrations of tritium already induce a significant amount of defects at short exposure times. Our findings are supported by molecular dynamics simulations of graphene bombardment with tritium atoms. As a consequence, tritium saturation of graphene may alter its permeability for hydrogen isotopes, thus affecting potential applications.

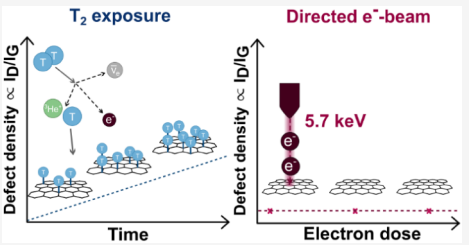




## 1. INTRODUCTION

**1.1. Background.** Nuclear fusion is deemed a promising perspective to help cope with the increasing demand for energy from sources with a low carbon footprint.[1] Tritium, the radioactive isotope of hydrogen, is supposed to be used as fuel in combination with deuterium. Furthermore, tritium is widely used as a tracer and in radiopharmaceutical synthesis.[2−5] On the other hand, it is a matter of concern as it is produced in fission reactors and can leak into the environment.[6−8] Especially for the commercial realization of nuclear fusion, the development of efficient tritium processing technologies is required. Among them, highly selective tritium separation methods need to be explored.

A multitude of methods exist to separate and purify hydrogen from multicomponent mixtures, e.g., electrochemical methods.[9,10] In recent works the selective adsorption on microporous materials, but also the selective diffusion/permeation through proton-conducting polymer membranes proved to be promising for the separation of hydrogen isotopes.[11−13] For these, graphene was additionally used to increase the separation efficiency.[14]

Graphene, first synthesized and identified in 2004, is a two-dimensional carbon monolayer with a hexagonal structure, featuring extraordinary properties.[15,16] These include very high electron mobility, a high optical transparency and high mechanical stability.[17−19] Furthermore, it is generally impermeable for gas molecules.[20] The characteristics of graphene can be modified, e.g., via doping or through the "engineering" of defects.[21] It is also possible to modify the structure by hydrogenation leading to graphane structures.[22−25] In a recent study in the field of experimental astroparticle physics, Zeller et al. demonstrated the possibility of tritium adsorption on graphene.[26] Tritiated graphene is also considered for use in the PTOLEMY experiment, in which it serves as a target for capturing relic neutrinos.[27]

The interaction between tritium and graphene leads to the question of whether the graphene structure is modified and what kind of modification might be observed. In view of possible applications for isotope separation, structural changes could impact the selectivity after prolonged and repeated tritium exposure. In a first experiment, Xue et al. were able to separate tritium from water using proton exchange membrane water electrolysis (PEMWE), but attributed the high selectivity to the used catalyst, not to the graphene.[28] Tritiated water has not been found to change the graphene structure.[29] However, for gaseous tritium, with its high activity concentration and insignificantly moderated beta particles, the impact of exposure is likely to be more striking.

**1.2. Defects in Graphene.** The occurrence of defects in graphene structures is intensively studied, cf. Table S1 Supporting Information for an overview of the most commonly

Received: June 19, 2025
Revised: October 27, 2025
Accepted: October 28, 2025
Published: December 2, 2025

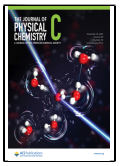





https://doi.org/10.1021/acs.jpcc.5c04255
J. Phys. Chem. C 2025, 129, 21995−22005

observed defects. Some defects can be introduced during the growth of the lattice, such as grain boundary defects.[30] The structure can also be altered by chemical modifications, such as doping as well as hydrogenation.[21,25] It has been found that vacancy defects are able to migrate through the graphene structure.[31] Additionally, it has been shown that the graphene structure is altered as a result of electron irradiation.[32]

The most abundant defect type is the Stone−Wales (SW) defect, in which the bond between two carbon atoms has been rotated by 90°, thus forming two 5-rings and two 7-rings.[33] The SW defect has been theorized to aid in hydrogen isotope separation.[34]

**1.3. Identification of Defect Structures in Graphene.** For analyzing the quality of graphene, one of the most common methods is Raman spectroscopy, due to the characteristic spectrum consisting of the so-called G- and 2D-bands, at ∼1580 $cm^{-1}$ and ∼2700 $cm^{-1}$, respectively.[35] With an increase in defects, the D-band emerges.[36] Thus, the intensity ratio between the D- and the G-band can be used to evaluate the defect evolution in graphene.[37] Additionally, the method is nondestructive, allowing further analysis of the samples.

Another method is transmission electron microscopy (TEM), which can visualize defects while generating them by electron bombardment during the measurement.[38] It can be used to image defects at the atomic level, showing the characteristic structures of, e.g., Stone−Wales defects or vacancies.[39] Scanning tunneling microscopy (STM) is also a suitable method for graphene imaging.[40] X-ray photoelectron spectroscopy (XPS) has been used to measure structural changes, e.g., induced by dopants.[41,42] These methods were not used in this work, because the handling of tritium-containing samples requires specific equipment.

**1.4. Experimental Approach.** As it was first demonstrated by Zeller et al., the exposure of graphene to tritium leads to chemical adsorption of tritium as well as to vacancy-type defects.[26] However, it remained unclear how the vacancy defects are created. Changes in the graphene structure can potentially be caused by beta electrons or by reactive tritium species formed by beta decay. In addition, the beta decay of tritium produces $^3He$ in various charge states (neutral $^3He$, $^3He^+$, $^3He^{2+}$, and molecular ions). However, helium-induced damage to graphene is typically reported for keV-scale $He^+$ irradiation.[43] This is far above the eV-scale recoil energies from tritium beta decay.[44] Therefore, helium is not considered as primary driver of defects. The respective impact of the other two mechanisms on structure changes of graphene is unknown and needs to be studied. On the one hand, we irradiated graphene samples in a SEM with 5.7 keV electrons, which correspond to the average kinetic energy of the tritium decay electrons. Furthermore, we investigated if exposure to tritium gas at comparable electron doses impacts the graphene structure in the same fashion as electrons do.

To provide a more in-depth perspective into the energetics and kinetics of the formation of different defect types, we employed computational studies. These allowed us to predict the defect behavior under various conditions and to characterize the interaction of tritium with graphene as a function of both energy and defect presences.

## 2. MATERIALS AND METHODS

**2.1. Graphene Samples.** Irradiation and measurements were conducted with 5 mm × 5 mm monolayer graphene samples on a $Si/SiO_2$ substrate (ACS Material LLC, Pasadena, USA) (Figure S2). The graphene was placed on the substrate by the manufacturer using their proprietary *Trivial Transfer Graphene*.[45] The copper substrate on which the graphene is grown is typically removed by etching. To stabilize the graphene during this process, and to easily transfer it to the new substrate, a coating of poly(methyl methacrylate) (PMMA) is applied and dissolved after transfer.[46]

**2.2. Oriented Irradiation: Raster Scanning of Surface Using SEM.** Four graphene samples have been electron-irradiated inside a scanning electron microscope (EVO-50, Zeiss, Oberkochen, Germany), equipped with a tungsten filament. The scanning was performed over an area of 2 mm × 2 mm, using a defocused electron beam to ensure uniform irradiation. The acceleration energy was set to 5.7 keV, as this corresponds to the average energy of the electrons emitted by tritium decay. The constant beam current was set to (10 ± 3) nA. It should be noted that the actual beam current generally depends on the SEM gun setup. Different electron doses were applied, calculated from the beam current and irradiation duration. The samples were irradiated for 1.00, 2.02, 2.68, and 4.05 h, respectively. All SEM irradiation conditions are summarized in the Supporting Information Table S2.

**2.3. Direct Exposure to Gaseous Tritium.** We made an estimate whether the number of electrons that interact with the graphene under tritium exposure is comparable to pure electron irradiation. During the tritium chamber irradiation, the number of primary, backscattered and secondary electrons passing through the graphene layer was calculated using the CASINO software package for scanning electron microscopy.[47] To facilitate an estimation, the geometry of the tritium chamber was simplified as a 2 mm spacing between two infinitely extended walls of stainless steel and the $SiO_2$ substrate. Furthermore, it was neglected that the electrons from tritium upon decay have an energy distribution, as this cannot be considered using the CASINO software.

The resulting estimation predicts that out of 100 electrons generated in the tritium gas, the number of electrons passing through the graphene layer is around 55 (primary and backscattered electrons), plus an additional 41 secondary electrons originating from the $SiO_2$ substrate. Thus, the number of electrons interacting with the graphene is in the same order of magnitude as in the case of SEM irradiation, which justifies a comparison of electron doses calculated from beam current and tritium activity. The exposure durations (22.89, 45.78, 68.68, and 91.57 h) were set on this basis.

To expose the graphene samples to tritium gas, a gastight setup was used to exclude any discharge of radioactive material. This was achieved by using a stainless steel vacuum compartment system (RC TRITEC, Teufen, Switzerland). An exposure cell with a volume of 5 mL was attached to the system (Figure S1). Four samples were treated at durations of 22.89, 45.78, 68.68, and 91.57 h, respectively, at room temperature and a tritium pressure of 100 mbar, amounting to approximately 44 GBq tritium. The doses applied by SEM irradiation correspond roughly to only the number of primary decay electrons, not including secondary effects.

**2.4. Confocal Raman Microscopy.** The Raman measurements were performed at the Tritium Laboratory Karlsruhe (TLK) with a confocal Raman microscope (CRM) that was specifically built for the measurement of toxic or radioactive samples.[48] All measurements were carried out with the same configuration using a 532 nm laser with a power of 120 mW.


https://doi.org/10.1021/acs.jpcc.5c04255
J. Phys. Chem. C 2025, 129, 21995−22005

This corresponds to a power density on the graphene surface of about $3 \times 10^5$ W/cm$^2$. At this power density, the graphene layer is not damaged even after many hours of exposure to the laser beam.

The spectrometer of the CRM was equipped with a 1200 g/mm grating, resulting in a resolution of $(9.6 \pm 0.7)$ cm$^{-1}$. For the spectra presented in this work, no spectral sensitivity calibration of the detection system was performed. Therefore, only qualitative comparisons to literature data are possible, also due to the fact that in most of the literature, no statement about the intensity calibration of the used Raman system is made. The data within this work can, however, be compared quantitatively, since only relative changes are discussed, which are not affected by the intensity calibration.

For the used graphene samples, the measured Raman signal was about 300 times weaker than for previously measured samples provided by Graphenea, used by Zeller et al.[26] In comparative measurements against samples by other suppliers, it was demonstrated that the weak signal can be related to the sample quality and not to the specific measurement. Bright-field microscopy revealed dark lines and structurally damaged regions, which reduced effective collection efficiency/coverage and thus lower the absolute Raman signal (cf. Figure S2). This necessitated a considerably increased acquisition time for every single spectrum of 300 s and averaging of multiple consecutive spectra (10−20) to obtain an acceptable signal-to-noise ratio.

As a consequence, raster scanning of the graphene samples was impractical, and the data analysis required additional steps, especially regarding the increased number of cosmic ray signals and background fluorescence in each spectrum. To remove the cosmic rays, we used a modified z-score based algorithm, which was applied two consecutive times.[49] Afterward, the spectrum was smoothed using the Savitzky−Golay filter from the SciPy library.[50−52] The background fluorescence was removed. For this purpose, a baseline estimation was performed using an asymmetric least-squares smoothing algorithm.[51] The remaining constant background was subtracted. Seven peaks (D-, G-, D′-, and 2D-peak of graphene, $N_2$-, $O_2$-, and Si-3TO-lines) in the spectra were fitted simultaneously with Lorentzian functions.[53]

**2.5. Heating of Exposed Tritium Samples.** The motivation for the bake-out of the graphene samples was to quantify the activities in terms of the amount of bound radiolytic tritium. Using a tritium compatible oven, activities released from the graphene samples were measured. In short, the exhaust from the oven, mostly $T_2$ and HTO, passes through an oxidizing CuO-wire bed with a jacket heater operated at 450 °C, and then through a water bubbler, where all tritiated species are retained. The content of the water bubbler is then analyzed by liquid scintillation counting (LSC) to determine the total activity released during the sample heating. The completeness of recovery was recently demonstrated.[54] All four tritiated samples were heated at 300 °C for 3.5 h in a stream of argon gas. Time and temperature were chosen for comparability to the investigations by Zeller et al.[26]

**2.6. Theoretical Approach to the Interaction between Graphene and Tritium.** To better understand the experimental results and the changes in the graphene structure upon exposure to tritium, we performed molecular mechanics simulations of tritium bombardment of graphene with varying kinetic energies. We simulated the adsorption, transmission (penetration), and reflection rates of tritium atoms on graphene, employing the Large-scale Atomic/Molecular Massively Parallel Simulator (LAMMPS).[55] We investigated the tritium bombardment on pristine, Stone−Wales 555−777, and 5−8−5 divacancy defective graphene. We employed molecular dynamics (MD) simulations within a $7 \times 7 \times 1$ supercell of pristine graphene and within a $12 \times 12 \times 1$ supercell of defective graphene. The interactions between carbon atoms were modeled using two potentials, Reactive Empirical Bond Order (REBO)[56] and the Adaptive Intermolecular Reactive Empirical Bond Order (AIREBO) potential.[57] To obtain the adsorption, transmission, and reflection rates for tritium atoms with a certain kinetic energy, from 5 to 100 eV (with steps of 5 eV) for AIREBO and from 1 to 15 eV (with steps of 1 eV) for REBO, we placed a grid of tritium atoms 4 Å above the layer of graphene and we ran 1000 MD steps, with 0.1 fs time steps, at 400 K, employing the NVT ensemble with the fixed kinetic energy. Incident energies lower than 5 eV were not considered due to an inconsistency of the AIREBO potential. However, it is expected that when the incident kinetic energy increases, the transmission probability increases.

We created different grids of tritium atoms above pristine and defective graphene models, with 995, 2297, and 1221 tritium atoms for pristine, Stone−Wales 555−777, and 5−8−5 divacancy defective graphene, respectively. Each grid point shows the initial position of the tritium atoms with respect to the graphene layer and was calculated as a separate MD trajectory. The adsorption, reflection, and transmission of tritium atoms were classified according to the final distance of the atoms from graphene.

Additionally, we employed metadynamics simulations to investigate the free energy profile of the formation and transformation of Stone−Wales (SW) defects in a graphene monolayer. These simulations were also conducted using LAMMPS and the AIREBO potential.[55,57] The details of the metadynamics simulations are shown in the Supporting Information.

## 3. RESULTS AND DISCUSSION

Pristine graphene has two characteristic Raman bands: the 2D-band at ∼2700 cm$^{-1}$ and the G-band at ∼1580 cm$^{-1}$, as shown in Figure 1. These bands are associated with phonon modes in the absence of defects in the graphene layer. More specifically,

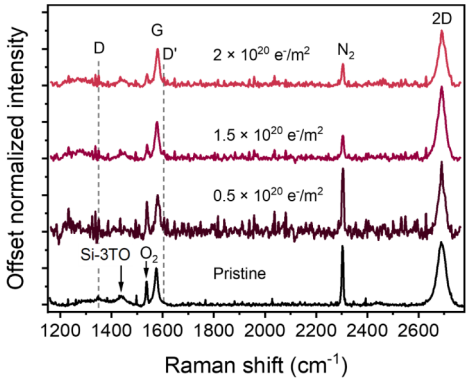


**Figure 1.** Evolution of representative Raman spectra with increasing electron doses. The spectra are normalized to their respective G-band amplitudes. Due to the weak Raman signal from these particular samples and the increased measurement times, $O_2$ and $N_2$ as well as the third order transverse-optical silicon band (Si-3TO) are visible in the spectra.



https://doi.org/10.1021/acs.jpcc.5c04255
J. Phys. Chem. C 2025, 129, 21995−22005

an intensity ratio of $I_{2D}/I_G > 2$ is associated with high-quality defect-free graphene. When defects are present in a graphene layer, additional peaks are observed, the most important being the D-band at ~1340 $cm^{-1}$. In the low-defect regime (referred to as Stage 1), the intensity ratio $I_D/I_G$ is directly proportional to the defect density and should be close to zero for defect-free graphene.[37,58] Some pristine graphene materials show a D-peak because of defect structures introduced during synthesis.[59] The $I_D/I_G$ ratio from one of our untreated samples (cf. Figure 1) was determined to be 0.2. As shown in Figure S2, the graphene samples, although untreated, show visible defects, which likely lead to this slightly increased intensity ratio.[60] With the employed confocal Raman microscope, there is no way to detect and avoid these defects since it does not have the functionality of a light microscope. Therefore, in this work any $I_D/I_G \leq 0.2$ can be attributed to edge defects and grain borders.

In general, a distinction is made between the low-defect regime (Stage 1) and the high-defect regime (Stage 2) of graphene. Starting from defect-free graphene, the $I_D/I_G$-ratio increases as the defect density increases. At a certain threshold of the defect density, the $I_D/I_G$-ratio reaches a maximum. This defines the transition from Stage 1 to Stage 2. As the defect density continues to increase, the $I_D/I_G$-ratio as well as the overall intensities of all Raman bands decrease.[37,60] Therefore, when discussing and comparing $I_D/I_G$-ratios and corresponding defect densities, it needs to be considered if the graphene sample is in Stage 1 or Stage 2. Using additional spectral information, e.g., the width of the D-, G- or 2D-band, this ambiguity can be resolved.[61,62]

Additional bands in defective graphene are the D′-band at ~1620 $cm^{-1}$ and the G+D-band at ~3000 $cm^{-1}$. Of particular interest is the D′-band, because the intensity ratio $I_D/I_{D'}$ is sensitive to the different types of defects in graphene. In graphene with only $sp^3$-type defects, $I_D/I_{D'}$ is ~13, meaning the D′-peak is relatively small. In the presence of mainly vacancy-type defects, $I_D/I_{D'}$ is ~7, thus the D′-peak is comparatively larger. Due to the weak Raman signal of the particular graphene samples used for this work, the D′-peak can only be fitted with large uncertainty, and the resulting intensity was compatible with zero in all cases. However, in this work we are only concerned with the total amount of defects created by either electron irradiation or tritium exposure and not with fingerprinting the defect types, as we are investigating the role of the beta electrons during tritium exposure.

**3.1. Changes in the Graphene Structure Caused by Electron Irradiation.** Figure 1 shows the Raman spectra of the graphene samples that were exposed to electron irradiation by an SEM. The full summary of the fit results is reported in the Supporting Information (cf. Tables S4, S5, S6). The spectral features show only negligible differences for the increasing electron dose from $0.5 \times 10^{20}$ to $2 \times 10^{20}$ $e^-/m^2$. Specifically, the normalized intensities and widths of the G-peak and the 2D-peak remain unchanged within the uncertainties of the fit. The spectra show no D-peak, even with increasing electron doses, indicating that no or only few defects have been generated by the SEM irradiation. This also indicates that these measurements were conducted on an edge-defect-free area. Instead of the $I_D/I_G$ peak ratio, the noise-to-G-peak ratio was determined for all measured spectra with an average of 0.12 (Table 1). (The measurement of the sample exposed to an electron dose of $1.0 \times 10^{20}$ $e^-/m^2$ failed because of a defect on the Raman laser.) To assess possible manufacturer-dependent effects, we repeated the irradiation on graphene from a different manufacturer (Graphenea, San Sebastian, Spain) at 5.6, 10, 20, and 30 keV with doses of 1.5, 2.0, 5.0, 10.0, $15.0 \times 10^{20}$ $e^-/m^2$. Again, no significant D-peak was observed. The corresponding spectra are provided in the Supporting Information (cf. Figure S4).

**Table 1. Noise-to-Peak Ratios for the SEM Irradiated Graphene Samples**[a]

| Electron dose | Noise-to-peak ratio |
|---|---|
| Pristine | 0.12 |
| $0.5 \times 10^{20}$ $e^-/m^2$ | 0.20 |
| $1.5 \times 10^{20}$ $e^-/m^2$ | 0.09 |
| $2.0 \times 10^{20}$ $e^-/m^2$ | 0.08 |

[a]The noise level was determined as the standard deviation for each spectrum at (1350 ± 40) $cm^{-1}$ and was divided by the intensity of the measured G-peak.

Figure 2 shows an overview plot of results from literature as well as results from this work. In the literature, higher $I_D/I_G$-ratios of up to $I_D/I_G = 1$ were reported at similarly low doses. However, studies reported in the literature employed electron energies above 10 keV. As outlined above, the curves show distinctive trends, first increasing with higher electron doses and then decreasing again. For our work, only low electron doses were of interest. Noticeably, the highest $I_D/I_G$-ratios were observed at 10 keV, with a lower maximum ratio at 30 keV and even lower at 20 keV. Additional literature suggests that changes in the spectra, and thus $I_D/I_G$, may not solely result from amorphization at such low energies, but at least partially from hydrogenation or surface contamination, which can be removed by annealing.[63,64] Tao et al. have reported a small blue shift in the Raman spectra after annealing, indicating a structural modification.[64] It has also been suggested that

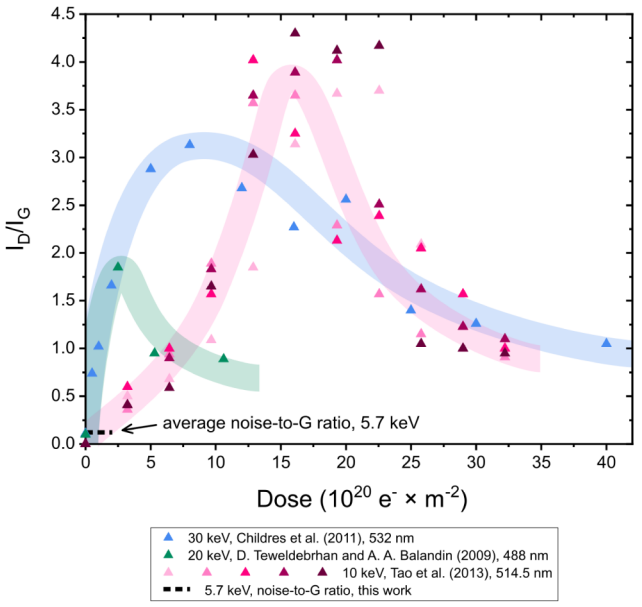


**Figure 2.** Compilation of the $I_D/I_G$ (indicator of defect density) ratio data after SEM irradiation in relation to electron dose. Extracted literature data for 10 keV (pink to magenta), 20 keV (green) and 30 keV (blue) are compared with data from this study (black).[64,67,68] The stated wavelengths refer to the applied laser beams used. Colored bands have been added to guide the eye.



https://doi.org/10.1021/acs.jpcc.5c04255
J. Phys. Chem. C 2025, 129, 21995−22005

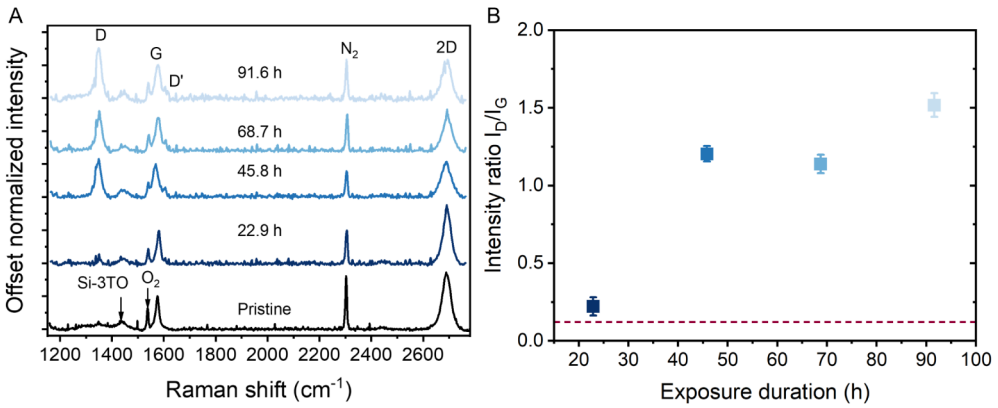


**Figure 3.** (A) Evolution of representative Raman spectra with increasing time of exposure to tritium. (B) Evolution of the intensity ratio $I_D/I_G$ as an indicator of changes in the defect density. The red line indicates the average noise-to-G-peak ratio observed after electron irradiation, as shown in Figure 1 and Table 1. The spectra were normalized to the respective G-band amplitudes.

defects, as visible from Raman spectra, stem from radical compounds formed within the electron beam, leading to chemical etching.[38] Some low-energy e-beam studies likewise find that few-keV electrons primarily cause reversible adsorbate-related spectral changes rather than permanent lattice damage.[65] Moreover, creating vacancies via knock-on requires on the order of ∼80 keV imparted to a carbon atom, which is not reached under our e-beam conditions.[66] Therefore, our observation that a 5.7 keV electron beam does not modify the graphene structure is not unexpected.

In summary, we conclude that the oriented beam of 5.7 keV electrons, which mimics the exposure to electrons released by the beta decay of tritium, does not modify the graphene structure.

**3.2. Effect of Exposure to Gaseous Tritium.** Four individual graphene samples were exposed to tritium gas at a constant pressure (100 mbar) in a constant volume (5 mL). Only the exposure time was varied. The corresponding Raman spectra of the graphene samples after each exposure are shown in Figure 3A. In general, it can be observed that the D-band intensity increases with longer exposure times, while the 2D-band intensity slightly decreases. Both observations indicate an increasing degradation of the graphene layer. The intensity ratio $I_D/I_G$, which is directly proportional to the defect density in Stage 1 is shown in Figure 3B.

After 22.9 h of exposure to tritium, the changes in the Raman spectra are minimal compared to pristine graphene. The intensity ratio $I_D/I_G$ is less than 0.25, comparable to many pristine samples in the literature.[26,48] The same is true for the intensity ratio $I_{2D}/I_G$ (∼1.7). The $I_D/I_G$-ratio is only slightly higher than the noise-to-peak ratio observed for the SEM irradiated samples (cf. Figure 1). For the sample that was exposed to tritium for 45.8 h, a significant change in the Raman spectra can be observed, namely an increase of the D-peak and a decrease of the 2D-peak, leading to an $I_D/I_G$ of ∼1.2 and an $I_{2D}/I_G$ of ∼1.1. The samples that were exposed to tritium for 45.8 and 68.7 h show very little difference in the respective Raman spectra. Both intensity ratios remain unchanged within the stated uncertainties of the fit. Follow-up studies are needed to determine whether this small change in $I_D/I_G$ is reproducible. It cannot be excluded that the data point at 45.8 h could be an outlier caused by a morphological difference in this particular sample, as described below. After 91.6 h, the D-peak is further enhanced with an $I_D/I_G$ of ∼1.5. However, the intensity of the 2D-peak has not decreased significantly, indicating that the general structure of the graphene layer is still intact, which is expected behavior in Stage 1 (region of low-defect graphene).[69]

Note that in general sample morphology with preexisting defects can affect local sticking probabilities of tritium atoms, as discussed in Section 3.4, and thus could affect the evolution of the defect density as shown in Figure 3B. With the samples used in this work, there are two main indicators that there could be preexisting defects, namely (i) large-scale macroscopic heterogeneity (cf. Figure S2), and (ii) severely reduced Raman signal as compared to other monolayer graphene samples. However, these considerations do not alter the aim of this study, which is to disentangle the role of beta decay electrons from that of reactive tritium species in defect formation. To assess robustness with respect to preexisting defects, we additionally simulated tritium-graphene interaction on both pristine and defective graphene (see Figure 6).

Although the Raman signal of these graphene samples is relatively weak and the D′-peak cannot be fully resolved, the spectra are consistent with a modest concentration of $sp^3$-type defects, i.e., a covalent bond between a tritium atom and the carbon of the graphene layer.[62,69] As the defect assignment is based on the $I_D/I_{D'}$ intensity ratio, $sp^3$-type functionalization typically yields a higher $I_D/I_{D'}$, whereas vacancy-type defects tend to give a comparatively stronger $I_{D'}$ and thus a lower ratio. Given the limited $I_{D'}$ resolvability here, we refrain from a quantitative estimate and treat the assignment as tentative.

**3.3. Released Activity from Graphene Samples.** Although it cannot be easily quantified how much of the tritium is adsorbed on graphene and how much is absorbed in the $SiO_2$/Si substrates, the released activity after bake-out provides a quantitative metric characterizing the different loading experiments. Because all samples used the same substrate and fabrication, any substrate contribution should be comparable across samples.

Figure 4 shows the released activity $A_R$ as a function of (A) the total decays that occurred during the exposure time within the chamber volume in a log−log plot, and (B) the decay density in the chamber volume in a log−linear plot. Data points from Zeller et al.[26] are included as open circles. As the area of samples used in the aforementioned study was larger, a correction factor of 0.25 was applied to the released activity value from Zeller et al. For both plots a linear fit was performed as shown.



https://doi.org/10.1021/acs.jpcc.5c04255
J. Phys. Chem. C 2025, 129, 21995−22005

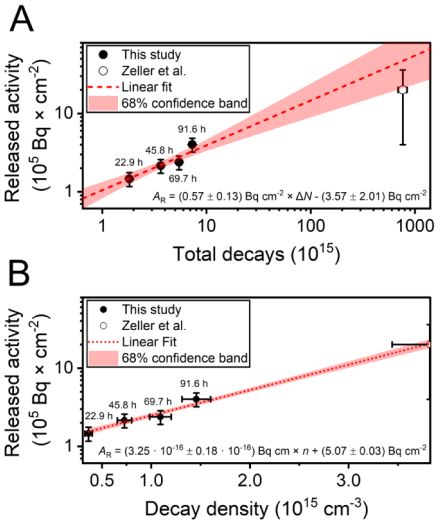


**Figure 4.** Activities released after the bake-out of the graphene samples (on Si/$SiO_2$ substrate), corresponding to the amount of radiolytically available tritium. The exposure times of each measured sample are indicated at the data points. Open points indicate data from Zeller et al.[26] (A) Plot as a function of the total decays in the chamber during the exposure time. (B) Plot as a function of the decay density during the exposure time. The calculations and exact values are given in the Supporting Information (Table S3). In the fit equations, $A_R$ denotes the released activity, $\Delta N$ is the total number of decays, and $n$ is the decay density.

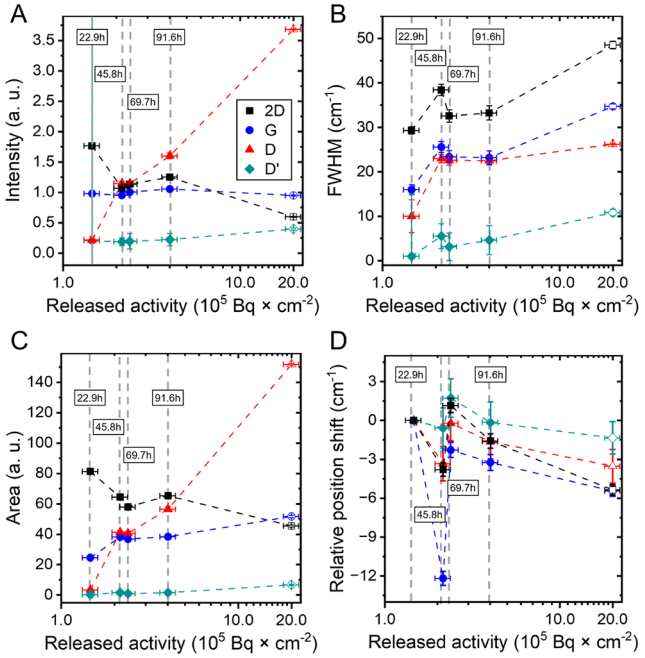


**Figure 5.** Different Raman spectrum peak parameters vs released activity from graphene on Si/$SiO_2$ samples after heating. (A) Evolution of the peak intensities, (B) changes in the full width at half maximum (FWHM) of the peaks, (C) evolution of the peak areas, (D) changes in the relative peak position shift with increasing released activity. The exposure durations are indicated for data points from this work for easier referencing in the main text. Peaks are identified in the legend of panel A. Open points indicate data from Zeller et al.[26] The dashed lines provide guides to the eye. Note the large error of the D′-peak is caused by the uncertainties of the fit.

We want to highlight that compared to the exposure applied by Zeller et al., the total number of decays in this work is 2 orders of magnitude smaller (Figure 4A).[26] However, the decay density, based on the volume of the exposure cells, differs only by a factor of about 2.5 (Figure 4B). In the following, we use the released activity $A_R$ as a common parameter as we assume that $A_R$, up to a proportionality factor and/or offset, is related to the adsorbed activity on the graphene samples and thus also to the defect density in the graphene samples.

$A_R$ is used in Figure 5 to compare the results from this work and the results from Zeller et al. The charts show the peak intensity, peak area, FWHM, and a relative position shift of the main Raman peaks of graphene (2D, G, D, and D′). Note that the data is normalized to the intensity of the G-peak as in Figure 3. Therefore, the intensities shown in Figure 5A can be interpreted relative to the G-peak as $I_D/I_G$, $I_{2D}/I_G$ and $I_{D'}/I_G$. The full summary of the fit results is reported in the Supporting Information (cf. Tables S4, S5, S6).

As it was described previously, the $I_D/I_G$-ratio is directly proportional to the defect density (here estimated by $A_R$) in graphene in the low defect regime (Stage 1). Note that with increasing $A_R$, the D-peak intensity and area (Figure 5C) increases. The $I_D/I_G$-ratio should reach a global maximum at a threshold value of $A_R$, followed by a decrease in the $I_D/I_G$-ratio with further increasing $A_R$. Due to the relatively increased fwhm of all peaks (Figure 5B) it can be concluded that the graphene samples from Zeller et al. (data points at $A_R \cong 20 \times 10^5$ Bq/cm$^2$ correspond to the high-damage density regime of graphene (Stage 2). Therefore, the predicted maximum of the D-peak intensity would most likely occur in the region between $A_R \cong 5 \times 10^5$ Bq/cm$^2$ and $A_R \cong 20 \times 10^5$ Bq/cm$^2$.

Noticeably, no significant differences are observed between the trends of the peak intensities (A) and peak areas (C). In both cases, the D-peak value increases with increasing $A_R$, while the 2D-peak value decreases. The G-peak intensity remains approximately 1, as the spectra are normalized to the G-peak maximum. However, the G-peak area increases with increasing $A_R$, which is also reflected in the broadening of the G-peak (B). A significant increase in the D′-peak intensity and area is only visible for $A_R \cong 20 \times 10^5$ Bq/cm$^2$. For $A_R < 5 \times 10^5$ Bq/cm$^2$ it remains constant and small within the fit uncertainties. As discussed previously, the D′-peak is not fully resolved from the noise in this work, also leading to increased error bars of the fit results, most noticeable in Figure 5A. Regarding the peak widths (B), the FWHM of all four peaks increases with increasing $A_R$ except for the sample that was exposed to tritium for 45.8 h during this work. For this sample, all four peaks are significantly broadened. Thus, it appears to be an outlier. A similar effect can be observed when looking at the relative position shifts of the peaks (D). In general, there appears to be a linear anticorrelation between the shift and $A_R$ with the 45.8-h-sample posing an outlier. The G-peak is shifted drastically by −12 cm$^{-1}$. It is known that the G-peak position is blue-shifted in the case of both electron and hole doping.[70] A similar effect, due with smaller magnitude (∼5 cm$^{-1}$), can be observed for the 2D-peak as well. The line position of $N_2$ (see Figure 3) is stable within ± 2 cm$^{-1}$ across all measurements in this work, indicating that the blue shift is indeed a physical effect. As already described above it needs follow-up studies to determine if this effect is reproducible.

These results demonstrate a clear correlation between increasing tritium exposure (more total decays, higher decay densities) and the spectral features of the graphene samples.



https://doi.org/10.1021/acs.jpcc.5c04255
J. Phys. Chem. C 2025, 129, 21995−22005

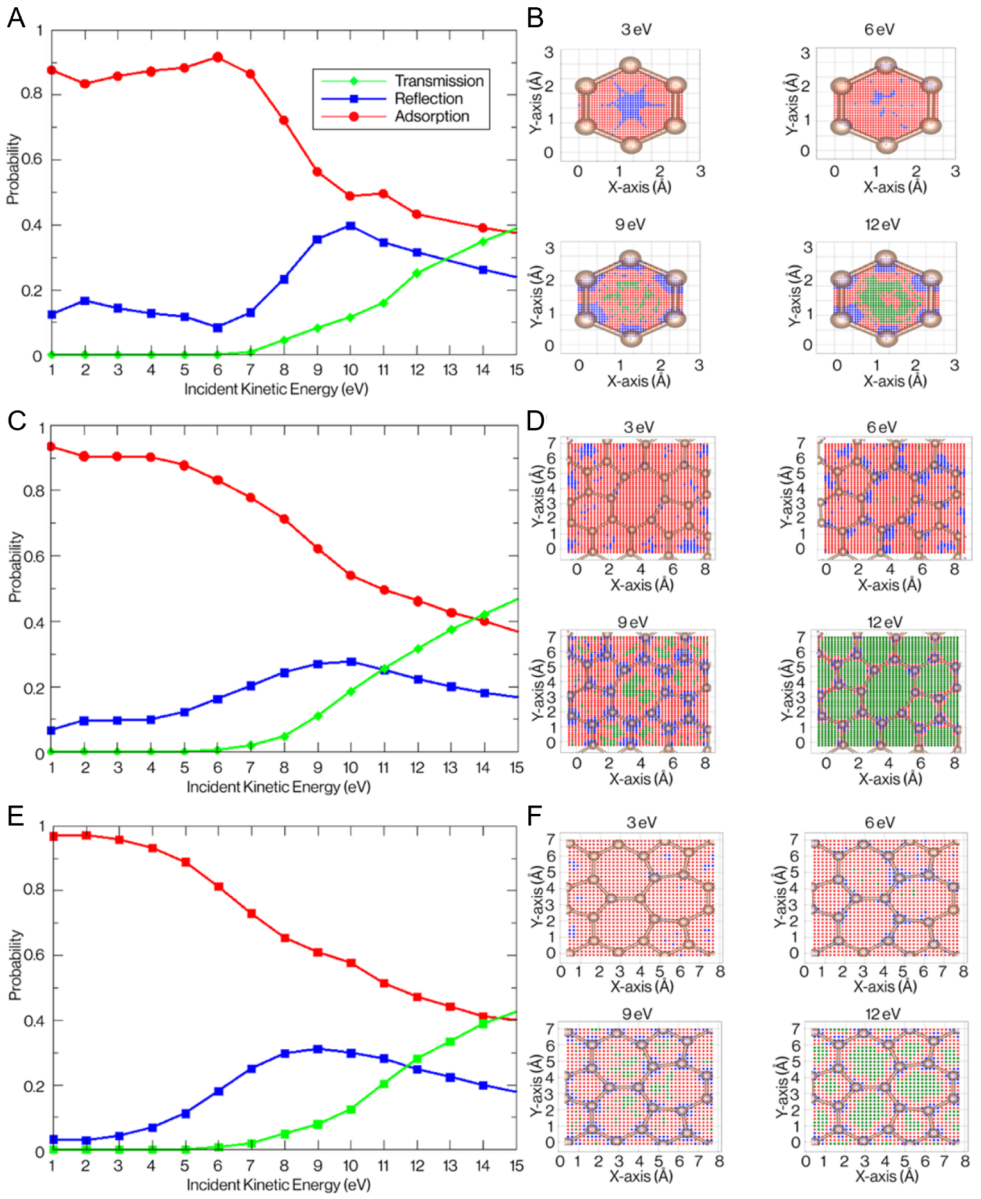


**Figure 6.** Single tritium interaction simulations conducted on pristine graphene, 5−8−5 divacancies, and 555−777 divacancy graphene structures using REBO potential. The probability of single tritium interaction is analyzed as a function of incident kinetic energy, considering transmission, adsorption, and reflection outcomes. Results are presented based on the initial exposure location: (A, B) for pristine graphene, (C, D) for 5−8−5 divacancy graphene, and (E, F) for 555−777 divacancy graphene.

The intensity and area ratios between the D- and G-peak increase, the peaks broaden and there are notable shifts in the peak positions. The results also indicate that with increasing tritium exposure, the released activity $A_R$ is increasing, which suggests that also the amount of adsorbed tritium is increasing. Furthermore, $A_R$ is indeed related to the defect density caused by tritium adsorption. Therefore, at least some amount of the released activity has to originate from the graphene layer itself and not only from the $Si/SiO_2$ substrate.

**3.4. Theoretical Investigation of Pre-existing Defects on the Interaction between Graphene and Tritium.** We have investigated by means of simulation what happens when pristine or defective graphene is exposed to tritium bombardment with various initial kinetic energies. The results are summarized in Figure 6, showing the adsorption, reflection, or transmission rates of tritium atoms. In general, increasing the kinetic energy increases the transmission probability and reduces the possibility to form C−T bonds or to reflect tritium atoms. In detail, there are two crossing points in Figure 6, which correspond to the crossing between the transmission and either reflection or adsorption. Both points are observed at higher kinetic energies of tritium in case of pristine graphene and are about 1−2 eV lower in energy for the defective systems, indicating that much less energy is needed to modify the existing defects than to form them from a pristine material. We calculated these processes with two different potentials, REBO (shown in Figure 6) and AIREBO shown in Figure S6. It is important to mention a few differences between the two methods: 1. The crossing points using REBO are closer in energy than those from AIREBO; 2. The trends at lower energies indicate that using AIREBO favors the reflection over the adsorption, which is not very intuitive. These differences come from the fact that AIREBO overestimates the Lennard-Jones interactions, thus, resulting in exaggerated repulsion,


https://doi.org/10.1021/acs.jpcc.5c04255
J. Phys. Chem. C 2025, 129, 21995−22005

especially visible at low kinetic energies. This was also observed by other researchers.[71] At very low energies (up to 4 eV), adsorption dominates, leading to the formation of C−T bonds, while the probability of reflection remains negligible. At high energies (above 20 eV), transmission becomes the primary process, whereas reflection is most significant at intermediate energies (5−20 eV). Our results agree very well with other theoretical studies.[71−74] A subtle distinction between pristine and defective graphene arises in the onset of reflection: in the defective system, the probability of reflection begins to increase at around 4−5 eV, compared to 6−7 eV for pristine graphene.

It is expected that below 5 eV kinetic energy the reflection is lower than adsorption. Additionally to defect formation, the C−T bonds are formed which should be observed in Raman spectra as D′-bands. On the other hand, for higher kinetic energies, the tritium transmission through graphene may result in C atoms knockout and vacancy formation or defect transformation, in case the tritium atoms are situated above C atoms. The increased formation of defects at higher kinetic energies should be reflected in the Raman spectra as an increased D-band.

The theoretical results show that in the low energy range ($\lesssim$ 20 eV) there is a certain probability ratio between adsorption and reflection of ∼2:1, which is rather unaffected by the existing defect type. This is an important aspect, as it suggests that differences in the tritium adsorption efficiency as a function of the defect type are unlikely to occur, and that strongly heterogeneous tritium adsorption behavior is not to be expected. Therefore, we can conclude that the presented results on tritiation are also applicable to graphene substrates that initially show a heterogeneous defect type distribution.

## 4. SUMMARY AND CONCLUSION

We exposed pristine graphene samples to radioactive tritium gas at a pressure of 100 mbar with different exposure times. In this gas, primary beta electrons (keV) as well as secondary particles from ionization and dissociation (low energy electrons, helium and tritium ions and atoms) are present. Our observations show that the interaction between graphene and tritium cannot be explained by electron irradiation alone. Using Raman microscopy, we observed a clear increase in defect density under tritium exposure and conclude that this increase cannot be accounted for by electron irradiation alone at comparable energies and doses.

The Raman-derived $I_D/I_G$-ratio indicates the general defect density, but due to poor signal-to-noise ratio, we cannot resolve the weak D′-peak signal and thus only have limited direct information about the defect type. Electron irradiation performed with an electron gun without an interfering gas atmosphere and thus absence of atomic or ionic species showed no significant changes in the Raman spectra and a vanishing D-peak. Literature data reports are in part contradictory: some studies[65] report no detectable Raman damage at comparable energies and doses, whereas others observe a pronounced D-peak only at substantially higher doses or higher-energy beams.[62,63,67] Consistent with the former, our electron-only controls showed no statistically significant spectral changes across 5.6−30 keV. It should also be noted that the median energy of the beta electron from tritium decay is even lower than 5.7 keV.

Due to tritium exposure, the defect density of graphene increases rapidly and at relatively low doses. Compared to previously investigated high electron doses, remarkably low concentrations of tritium already induce defects compatible with a mixture of adsorption-like ($sp^3$) and vacancy-like processes at exposure times as short as 22.9 h. Our tritium bombardment simulations show that there should be significant C−T bond formation (adsorption and formation of $sp^3$-C atoms) for lower kinetic energies of tritium atoms, while vacancy-type defects are formed for higher kinetic energies (transmission). Previous experiments have shown that the defect density increases with higher tritium exposure. As the $sp^3$-defects are attributed to tritiation, tritium saturation of the graphene may be at least partially possible. This could alter the electrochemical properties of graphene and affect hydrogen transport as well as selectivity in hydrogen isotope separation. Further research is needed to characterize the impact of the induced defects on physicochemical properties of graphene and thus on future applications of graphene membranes.

## ■ ASSOCIATED CONTENT

### Supporting Information

The Supporting Information is available free of charge at https://pubs.acs.org/doi/10.1021/acs.jpcc.5c04255.

Overview of defects in graphene, calculation of electron dose and total decays/decay density, electron irradiation and tritium exposure parameters, sketch of used setup, sample pictures, peak intensity and area ratios vs FWHM, additional theoretical investigations on defect formation and modification with metadynamics simulations (PDF)

## ■ AUTHOR INFORMATION


### Corresponding Author

**Alexandra Becker** − *Helmholtz-Zentrum Dresden-Rossendorf, Institute of Resource Ecology, Department of Reactive Transport, Leipzig 04318, Germany; Leipzig University, Faculty of Chemistry, Leipzig 04103, Germany;* orcid.org/0009-0004-2903-7242; Email: alexandra.becker@kit.edu

### Authors

**Genrich Zeller** − *Karlsruhe Institute of Technology, Institute for Astroparticle Physics, Tritium Laboratory Karlsruhe, Eggenstein-Leopoldshafen 76344, Germany;* orcid.org/0000-0002-9081-5582

**Holger Lippold** − *Helmholtz-Zentrum Dresden-Rossendorf, Institute of Resource Ecology, Department of Reactive Transport, Leipzig 04318, Germany*

**Ismail Eren** − *Helmholtz-Zentrum Dresden-Rossendorf, Institute of Resource Ecology, Department of Reactive Transport, Leipzig 04318, Germany; Helmholtz-Zentrum Dresden-Rossendorf, HZDR, Dresden 01328, Germany; Center for Advanced Systems Understanding, CASUS, Görlitz 02826, Germany*

**Lara Rkaya Müller** − *Federal Institute of Technology Zurich, Department of Chemistry and Applied Life Sciences, Zurich 8093, Switzerland*

**Paul Chekhonin** − *Helmholtz-Zentrum Dresden-Rossendorf, Institute of Resource Ecology, Department of Structural Materials, Dresden 01328, Germany*

**Agnieszka Beata Kuc** − *Helmholtz-Zentrum Dresden-Rossendorf, HZDR, Dresden 01328, Germany; Center for*




https://doi.org/10.1021/acs.jpcc.5c04255
J. Phys. Chem. C 2025, 129, 21995−22005

*Advanced Systems Understanding, CASUS, Görlitz 02826, Germany;* orcid.org/0000-0002-9458-4136
**Magnus Schlösser** − *Karlsruhe Institute of Technology, Institute for Astroparticle Physics, Tritium Laboratory Karlsruhe, Eggenstein-Leopoldshafen 76344, Germany*
**Cornelius Fischer** − *Helmholtz-Zentrum Dresden-Rossendorf, Institute of Resource Ecology, Department of Reactive Transport, Leipzig 04318, Germany; Leipzig University, Faculty of Chemistry, Leipzig 04103, Germany*

Complete contact information is available at: https://pubs.acs.org/10.1021/acs.jpcc.5c04255

### Author Contributions

Conceptualization: C.F., M.S., and A.K.; Data curation: A.B., G.Z., and I.E.; Formal analysis: A.B. and G.Z.; Funding acquisition: C.F. and A.K.; Methodology: A.B., G.Z., H.L., A.K., and P.C.; Project administration: C.F.; Resources: C.F., M.S., and A.K.; Software: L.R.M. and I.E.; Supervision: C.F., A.K., and M.S.; Visualization: A.B., G.Z., and I.E.; Writing − original draft: A.B., G.Z., I.E., P.C., and L.R.M.; Writing − review and editing: C.F., M.S., A.K., and H.L. All authors have given approval to the final version of the manuscript.

### Notes

The research data associated with this publication is available upon request in the RODARE repository under the DOI 10.14278/rodare.3733.
The authors declare no competing financial interest.

## ■ ACKNOWLEDGMENTS

The authors would like to thank Vanessa Dykas (HZDR) for her support with the graphene irradiation via SEM and Nancy Tuchscherer (KIT) for annealing of the tritium exposed graphene samples. We gratefully acknowledge funding from the Deutsche Forschungsgemeinschaft (DFG) − Project-ID 443871192 − GRK 2721 "Hydrogen Isotopes $^{1,2,3}$H", to C.F. and A.K.

## ■ REFERENCES

(1) Ongena, J. Nuclear Fusion and Its Large Potential for the Future World Energy Supply. *Nukleonika* **2016**, *61* (4), 425−432.
(2) Juhlke, T. R.; Sültenfuß, J.; Trachte, K.; Huneau, F.; Garel, E.; Santoni, S.; Barth, J. A. C.; Van Geldern, R. Tritium as a Hydrological Tracer in Mediterranean Precipitation Events. *Atmos. Chem. Phys.* **2020**, *20* (6), 3555−3568.
(3) Barešić, J.; Parlov, J.; Kovač, Z.; Sironić, A. Use of Nuclear Power Plant Released Tritium as a Groundwater Tracer. *Rud.-Geol.-Naftin Zb.* **2020**, *35* (1), 25−34.
(4) Atzrodt, J.; Derdau, V.; Kerr, W. J.; Reid, M. Deuterium- and Tritium-Labelled Compounds: Applications in the Life Sciences. *Angew. Chem., Int. Ed.* **2018**, *57* (7), 1758−1784.
(5) Lockley, W. J. S.; McEwen, A.; Cooke, R. Tritium: A Coming of Age for Drug Discovery and Development ADME Studies. *J. Label. Compd. Radiopharm.* **2012**, *55* (7), 235−257.
(6) Rethinasabapathy, M.; Ghoreishian, S. M.; Hwang, S.; Han, Y.; Roh, C.; Huh, Y. S. Recent Progress in Functional Nanomaterials towards the Storage, Separation, and Removal of Tritium. *Adv. Mater.* **2023**, *35* (48), 2301589.
(7) Weaver, C. L.; Harward, E. D.; Peterson, H. T. Tritium in the Environment from Nuclear Powerplants. *Public Health Rep.* **1969**, *84* (4), 363−371.
(8) Chae, J.-S.; Kim, G. Dispersion and Removal Characteristics of Tritium Originated from Nuclear Power Plants in the Atmosphere. *J. Environ. Radioact.* **2018**, *192*, 524−531.
(9) Amin, M.; Butt, A. S.; Ahmad, J.; Lee, C.; Azam, S. U.; Mannan, H. A.; Naveed, A. B.; Farooqi, Z. U. R.; Chung, E.; Iqbal, A. Issues and Challenges in Hydrogen Separation Technologies. *Energy Rep.* **2023**, *9*, 894−911.
(10) Lee, H. K.; Choi, H. Y.; Choi, K. H.; Park, J. H.; Lee, T. H. Hydrogen Separation Using Electrochemical Method. *J. Power Sources* **2004**, *132* (1−2), 92−98.
(11) Zhang, L.; Wulf, T.; Baum, F.; Schmidt, W.; Heine, T.; Hirscher, M. Chemical Affinity of Ag-Exchanged Zeolites for Efficient Hydrogen Isotope Separation. *Inorg. Chem.* **2022**, *61* (25), 9413−9420.
(12) Nam, J.; Cho, C.; Jung, S.; Jung, M.; Kim, Y.; Hong, Y.; Lee, S.; Oh, H.; Choe, W. High-Entropy Zeolitic Imidazolate Frameworks for Dynamic Hydrogen Isotope Separation. *Angew. Chem., Int. Ed.* **2025**, *64* (8), No. e202420379.
(13) Matsushima, H.; Ogawa, R.; Shibuya, S.; Ueda, M. Novel PEFC Application for Deuterium Isotope Separation. *Materials* **2017**, *10* (3), 303.
(14) Lozada-Hidalgo, M.; Zhang, S.; Hu, S.; Esfandiar, A.; Grigorieva, I. V.; Geim, A. K. Scalable and Efficient Separation of Hydrogen Isotopes Using Graphene-Based Electrochemical Pumping. *Nat. Commun.* **2017**, *8*, 15215.
(15) Novoselov, K. S.; Geim, A. K.; Morozov, S. V.; Jiang, D.; Zhang, Y.; Dubonos, S. V.; Grigorieva, I. V.; Firsov, A. A. Electric Field Effect in Atomically Thin Carbon Films. *Science* **2004**, *306* (5696), 666−669.
(16) Geim, A. K. Graphene: Status and Prospects. *Science* **2009**, *324* (5934), 1530−1534.
(17) Bolotin, K. I.; Sikes, K. J.; Jiang, Z.; Klima, M.; Fudenberg, G.; Hone, J.; Kim, P.; Stormer, H. L. Ultrahigh Electron Mobility in Suspended Graphene. *Solid State Commun.* **2008**, *146* (9−10), 351−355.
(18) Nair, R. R.; Blake, P.; Grigorenko, A. N.; Novoselov, K. S.; Booth, T. J.; Stauber, T.; Peres, N. M. R.; Geim, A. K. Fine Structure Constant Defines Visual Transparency of Graphene. *Science* **2008**, *320* (5881), 1308−1308.
(19) Lee, C.; Wei, X.; Kysar, J. W.; Hone, J. Measurement of the Elastic Properties and Intrinsic Strength of Monolayer Graphene. *Science* **2008**, *321* (5887), 385−388.
(20) Bunch, J. S.; Verbridge, S. S.; Alden, J. S.; Van Der Zande, A. M.; Parpia, J. M.; Craighead, H. G.; McEuen, P. L. Impermeable Atomic Membranes from Graphene Sheets. *Nano Lett.* **2008**, *8* (8), 2458−2462.
(21) Chen, W.; Chen, S.; Qi, D. C.; Gao, X. Y.; Wee, A. T. S. Surface Transfer P-Type Doping of Epitaxial Graphene. *J. Am. Chem. Soc.* **2007**, *129* (34), 10418−10422.
(22) Sofo, J. O.; Chaudhari, A. S.; Barber, G. D. Graphane: A Two-Dimensional Hydrocarbon. *Phys. Rev. B* **2007**, *75*, 15.
(23) Elias, D. C.; Nair, R. R.; Mohiuddin, T. M. G.; Morozov, S. V.; Blake, P.; Halsall, M. P.; Ferrari, A. C.; Boukhvalov, D. W.; Katsnelson, M. I.; Geim, A. K.; et al. Control of Graphene's Properties by Reversible Hydrogenation: Evidence for Graphane. *Science* **2009**, *323* (5914), 610−613.
(24) Jones, J. D.; Mahajan, K. K.; Williams, W. H.; Ecton, P. A.; Mo, Y.; Perez, J. M. Formation of Graphane and Partially Hydrogenated Graphene by Electron Irradiation of Adsorbates on Graphene. *Carbon* **2010**, *48* (8), 2335−2340.
(25) Pumera, M.; Wong, C. H. A. Graphane and Hydrogenated Graphene. *Chem. Soc. Rev.* **2013**, *42* (14), 5987.
(26) Zeller, G.; Díaz Barrero, D.; Wiesen, P.; Niemes, S.; Tuchscherer, N.; Aker, M.; Leonhardt, A. M. W.; Demand, J.; Valerius, K.; Bornschein, B.; et al. Demonstration of Tritium Adsorption on Graphene. *Nanoscale Adv.* **2024**, *6* (11), 2838−2849.
(27) Betti, M. G.; Biasotti, M.; Boscá, A.; Calle, F.; Cavoto, G.; Chang, C.; Cocco, A. G.; Colijn, A. P.; Conrad, J.; D'Ambrosio, N.; et al. Neutrino Physics with the PTOLEMY Project: Active Neutrino Properties and the Light Sterile Case. *J. Cosmol. Astropart. Phys.* **2019**, *2019* (7), 047−047.

(28) Xue, X.; Chu, X.; Zhang, M.; Wei, F.; Liang, C.; Liang, J.; Li, J.; Cheng, W.; Deng, K.; Liu, W. High Hydrogen Isotope Separation Efficiency: Graphene or Catalyst? *ACS Appl. Mater. Interfaces* **2022**, *14* (28), 32360−32368.
(29) Wang, W.; Zhou, M.; Yang, H.; Shao, Z. Radiation Resistance of Graphene in Tritiated Water. *Fusion Eng. Des.* **2024**, *200*, 114213.
(30) Lahiri, J.; Lin, Y.; Bozkurt, P.; Oleynik, I. I.; Batzill, M. An Extended Defect in Graphene as a Metallic Wire. *Nat. Nanotechnol.* **2010**, *5* (5), 326−329.
(31) Liu, L.; Gao, J.; Zhang, X.; Yan, T.; Ding, F. Vacancy Inter-Layer Migration in Multi-Layered Graphene. *Nanoscale* **2014**, *6* (11), 5729−5734.
(32) Girit, Ç. Ö.; Meyer, J. C.; Erni, R.; Rossell, M. D.; Kisielowski, C.; Yang, L.; Park, C.-H.; Crommie, M. F.; Cohen, M. L.; Louie, S. G.; et al. Graphene at the Edge: Stability and Dynamics. *Science* **2009**, *323* (5922), 1705−1708.
(33) Tiwari, S. K.; Pandey, S. K.; Pandey, R.; Wang, N.; Bystrzejewski, M.; Mishra, Y. K.; Zhu, Y. Stone−Wales Defect in Graphene. *Small* **2023**, *19* (44), 2303340.
(34) An, Y.; Oliveira, A. F.; Brumme, T.; Kuc, A.; Heine, T. Stone−Wales Defects Cause High Proton Permeability and Isotope Selectivity of Single-Layer Graphene. *Adv. Mater.* **2020**, *32* (37), 2002442.
(35) Ferrari, A. C.; Basko, D. M. Raman Spectroscopy as a Versatile Tool for Studying the Properties of Graphene. *Nat. Nanotechnol.* **2013**, *8* (4), 235−246.
(36) Chen, J.-H.; Cullen, W. G.; Jang, C.; Fuhrer, M. S.; Williams, E. D. Defect Scattering in Graphene. *Phys. Rev. Lett.* **2009**, *102* (23), 236805.
(37) Lucchese, M. M.; Stavale, F.; Ferreira, E. M.; Vilani, C.; Moutinho, M. V. O.; Capaz, R. B.; Achete, C. A.; Jorio, A. Quantifying Ion-Induced Defects and Raman Relaxation Length in Graphene. *Carbon* **2010**, *48* (5), 1592−1597.
(38) Krasheninnikov, A. V.; Nordlund, K. Ion and Electron Irradiation-Induced Effects in Nanostructured Materials. *J. Appl. Phys.* **2010**, *107* (7), 071301.
(39) Meyer, J. C.; Kisielowski, C.; Erni, R.; Rossell, M. D.; Crommie, M. F.; Zettl, A. Direct Imaging of Lattice Atoms and Topological Defects in Graphene Membranes. *Nano Lett.* **2008**, *8* (11), 3582−3586.
(40) Marchini, S.; Günther, S.; Wintterlin, J. Scanning Tunneling Microscopy of Graphene on Ru(0001). *Phys. Rev. B* **2007**, *76* (7), 075429.
(41) Panchakarla, L. S.; Subrahmanyam, K. S.; Saha, S. K.; Govindaraj, A.; Krishnamurthy, H. R.; Waghmare, U. V.; Rao, C. N. R. S. Structure, and Properties of Boron- and Nitrogen-Doped Graphene. *Adv. Mater.* **2009**, *21* (46), 4726−4730.
(42) Abdelnabi, M. M. S.; Blundo, E.; Betti, M. G.; Cavoto, G.; Placidi, E.; Polimeni, A.; Ruocco, A.; Hu, K.; Ito, Y.; Mariani, C. Towards Free-Standing Graphane: Atomic Hydrogen and Deuterium Bonding to Nano-Porous Graphene. *Nanotechnology* **2021**, *32* (3), 035707.
(43) Iberi, V.; Vlassiouk, I.; Zhang, X.-G.; Matola, B.; Linn, A.; Joy, D. C.; Rondinone, A. J. Maskless Lithography and in situ Visualization of Conductivity of Graphene Using Helium Ion Microscopy. *Sci. Rep.* **2015**, *5* (5), 11952.
(44) Schneidewind, S.; Schürmann, J.; Lokhov, A.; Weinheimer, C.; Saenz, A. Improved Treatment of the T2Molecular Final-States Uncertainties for the KATRIN Neutrino-Mass Measurement. *Eur. Phys. J. C* **2024**, *84*, 494.
(45) Materia ACS. *Graphene on Ultra-flat Thermal SiO2 Substrate*. https://www.acsmaterial.com/graphene-on-ultra-flat-thermal-sio2-substrate.html accessed 14−April−2025.
(46) Chaturvedi, P.; Moehring, N. K.; Knight, T.; Shah, R.; Vlassiouk, I.; Kidambi, P. R. The Parameter Space for Scalable Integration of Atomically Thin Graphene with Nafion for Proton Exchange Membrane (PEM) Applications. *Mater. Adv.* **2023**, *4* (16), 3473−3481.
(47) Demers, H.; Poirier-Demers, N.; Couture, A. R.; Joly, D.; Guilmain, M.; De Jonge, N.; Drouin, D. Three-dimensional Electron Microscopy Simulation with the CASINO Monte Carlo Software. *Scanning* **2011**, *33* (3), 135−146.
(48) Diaz Barrero, D.; Zeller, G.; Schlösser, M.; Bornschein, B.; Telle, H. H. Versatile Confocal Raman Imaging Microscope Built from Off-the-Shelf Opto-Mechanical Components. *Sensors* **2022**, *22* (24), 10013.
(49) Whitaker, D. A.; Hayes, K. A Simple Algorithm for Despiking Raman Spectra. *Chemom. Intell. Lab. Syst.* **2018**, *179*, 82−84.
(50) Savitzky, A.; Golay, M. J. E. Smoothing and Differentiation of Data by Simplified Least Squares Procedures. *Anal. Chem.* **1964**, *36* (8), 1627−1639.
(51) *PhD, N. C. Data Science for Raman spectroscopy Medium*. https://towardsdatascience.com/data-science-for-raman-spectroscopy-a-practical-example-e81c56cf25f accessed 31−January−2025.
(52) Virtanen, P.; Gommers, R.; Oliphant, T. E.; Haberland, M.; Reddy, T.; Cournapeau, D.; Burovski, E.; Peterson, P.; Weckesser, W.; Bright, J.; et al. SciPy 1.0: Fundamental Algorithms for Scientific Computing in Python. *Nat. Methods* **2020**, *17* (3), 261−272.
(53) *Data Fitting in Python Part II: Gaussian & Lorentzian & Voigt Lineshapes, Deconvoluting Peaks, and Fitting Residuals*; Emily Grace Ripka. http://emilygraceripka.com/blog/16. accessed 31−January−2025.
(54) Becker, A.; Lippold, H.; Bäcker, J. P.; Belder, D.; Fischer, C. An LSC Approach for Tritium Determination in Gaseous Mixtures Optimized with Respect to Handling, Reaction Parameters and Miniaturization towards Microfluidic Analysis. *Radiochim. Acta* **2024**, *112* (4), 231−237.
(55) Thompson, A. P.; Aktulga, H. M.; Berger, R.; Bolintineanu, D. S.; Brown, W. M.; Crozier, P. S.; In't Veld, P. J.; Kohlmeyer, A.; Moore, S. G.; Nguyen, T. D.; et al. LAMMPS - a Flexible Simulation Tool for Particle-Based Materials Modeling at the Atomic, Meso, and Continuum Scales. *Comput. Phys. Commun.* **2022**, *271*, 108171.
(56) Brenner, D. W.; Shenderova, O. A.; Harrison, J. A.; Stuart, S. J.; Ni, B.; Sinnott, S. B. A Second-Generation Reactive Empirical Bond Order (REBO) Potential Energy Expression for Hydrocarbons. *J. Phys.: Condens. Matter* **2002**, *14* (4), 783−802.
(57) Stuart, S. J.; Tutein, A. B.; Harrison, J. A. A Reactive Potential for Hydrocarbons with Intermolecular Interactions. *J. Chem. Phys.* **2000**, *112* (14), 6472−6486.
(58) Ferrari, A. C.; Meyer, J. C.; Scardaci, V.; Casiraghi, C.; Lazzeri, M.; Mauri, F.; Piscanec, S.; Jiang, D.; Novoselov, K. S.; Roth, S.; et al. Raman Spectrum of Graphene and Graphene Layers. *Phys. Rev. Lett.* **2006**, *97* (18), 187401.
(59) De Arco, L. G.; Zhang, Y.; Kumar, A.; Zhou, C. Synthesis, Transfer, and Devices of Single- and Few-Layer Graphene by Chemical Vapor Deposition. *IEEE Trans. Nanotechnol.* **2009**, *8* (2), 135−138.
(60) Casiraghi, C.; Hartschuh, A.; Qian, H.; Piscanec, S.; Georgi, C.; Fasoli, A.; Novoselov, K. S.; Basko, D. M.; Ferrari, A. C. Raman Spectroscopy of Graphene Edges. *Nano Lett.* **2009**, *9* (4), 1433−1441.
(61) Beams, R.; Gustavo Cançado, L.; Novotny, L. Raman Characterization of Defects and Dopants in Graphene. *J. Condens. Matter Phys.* **2015**, *27* (8), 083002.
(62) Eckmann, A.; Felten, A.; Verzhbitskiy, I.; Davey, R.; Casiraghi, C. Raman Study on Defective Graphene: Effect of the Excitation Energy, Type, and Amount of Defects. *Phys. Rev. B* **2013**, *88* (3), 035426.
(63) Teweldebrhan, D.; Balandin, A. A. Comment on "Modification of Graphene Properties Due to Electron-Beam Irradiation. *Appl. Phys. Lett.* **2009**, *94* (1), 013101.
(64) Tao, L.; Qiu, C.; Yu, F.; Yang, H.; Chen, M.; Wang, G.; Sun, L. Modification on Single-Layer Graphene Induced by Low-Energy Electron-Beam Irradiation. *J. Phys. Chem. C* **2013**, *117* (19), 10079−10085.

(65) Choi, J. H.; Lee, J.; Moon, S. M.; Kim, Y.-T.; Park, H.; Lee, C. Y. A Low-Energy Electron Beam Does Not Damage Single-Walled Carbon Nanotubes and Graphene. *J. Phys. Chem. Lett.* **2016**, *7* (22), 4739−4743.
(66) Ke, X.; Bittencourt, C.; Van Tendeloo, G. Possibilities and Limitations of Advanced Transmission Electron Microscopy for Carbon-Based Nanomaterials. *Beilstein J. Nanotechnol.* **2015**, *6*, 1541−1557.
(67) Teweldebrhan, D.; Balandin, A. A. Modification of Graphene Properties Due to Electron-Beam Irradiation. *Appl. Phys. Lett.* **2009**, *94* (1), 013101.
(68) Childres, I.; Foxe, M.; Jovanovic, I.; Chen, Y. P. Effect of Energetic Electron Irradiation on Graphene and Graphene Field-Effect Transistors. In *Micro- and Nanotechnology Sensors, Systems, and Applications III*; SPIE, 2011, Vol. *8038*, pp. 803122. .
(69) Eckmann, A.; Felten, A.; Mishchenko, A.; Britnell, L.; Krupke, R.; Novoselov, K. S.; Casiraghi, C. Probing the Nature of Defects in Graphene by Raman Spectroscopy. *Nano Lett.* **2012**, *12* (8), 3925−3930.
(70) Liu, J.; Li, Q.; Zou, Y.; Qian, Q.; Jin, Y.; Li, G.; Jiang, K.; Fan, S. The Dependence of Graphene Raman D-Band on Carrier Density. *Nano Lett.* **2013**, *13* (12), 6170−6175.
(71) Wu, E.; Schneider, C.; Walz, R.; Park, J. Adsorption of Hydrogen Isotopes on Graphene. *Nucl. Eng. Technol.* **2022**, *54* (11), 4022−4029.
(72) Taylor, S. S.; Skoufis, N.; Du, H.; Covington, C.; Varga, K. Hydrogen Adsorption and Scattering on Graphene with Electron Dynamics: Effects of Incident Point and Kinetic Energy. *Phys. Rev. A* **2025**, *112* (3), 032812.
(73) Ito, A.; Nakamura, H. Molecular Dynamics Simulation of Bombardment of Hydrogen Atoms on Graphite Surface. *Commun. Comput. Phys.* **2008**, *4* (3), 592−610.
(74) Ehemann, R. C.; Krstić, P. S.; Dadras, J.; Kent, P. R. C.; Jakowski, J. Detection of Hydrogen Using Graphene. *Nanoscale Res. Lett.* **2012**, *7* (7), 198.

## NOTE ADDED AFTER ASAP PUBLICATION

Due to a production error, a change was made to the second paragraph in section 2.3 after this article was published ASAP December 2, 2025. The corrected version was posted Decmeber 3, 2025.





https://doi.org/10.1021/acs.jpcc.5c04255
J. Phys. Chem. C 2025, 129, 21995−22005